# Role of matrix elements in the theoretical determination of generalized susceptibilities in metals*

Raju P. Gupta
*Magnetic Theory Group, Department of Physics, Northwestern University, Evanston, Illinois 60201*

A. J. Freeman
*Department of Physics, Northwestern University, Evanston, Illinois 60201*
*and Argonne National Laboratory, Argonne, Illinois 60439*

(Received 1 December 1975)

The role of matrix elements in the calculation of the generalized susceptibilities $\chi(\vec{q})$ of metals is discussed using the results of an augmented-plane-wave energy-band calculation for the eigenvalues and eigenfunctions of Sc metal. The inclusion of the oscillator strength matrix elements is found to significantly alter the structure obtained for $\chi(\vec{q})$ in the constant-matrix-element approximation. The effect of local-field corrections on the phonon anomaly in Sc and the observed magnetic ordering of dilute rare-earth Sc alloys are described; in the latter case, a crude estimate of this effect is found to restore a (broad) peak in $\chi(\vec{q})$ at $\vec{q} \approx [0,0,0.5(\pi/c)]$, in good agreement with experiment.

## I. INTRODUCTION

The generalized susceptibility function which measures the response of the system to an external probe is central to the understanding of many physical phenomena in solids. Although the calculations of these response functions are rather involved, the considerable refinement in the computational techniques which has been achieved in recent years makes accurate *ab initio* studies possible. The greater realization that (except perhaps for very simple metals) the true response function of a real solid is quite unlike the frequently used free-electron Lindhard function has led to attempts to include the real band-structure effects[1,2] into the calculations. In the random-phase approximation (RPA), the dynamic, i.e., wave-vector and frequency dependent, electron-electron dielectric function is written

$$\epsilon(\vec{q},\omega) = 1 + (4\pi e^2/\Omega q^2)\,\chi(\vec{q},\omega)\ , \tag{1}$$

where $\Omega$ is the crystal volume and

$$\chi(\vec{q},\omega) = \chi_1(\vec{q},\omega) + i\chi_2(\vec{q},\omega) \tag{2}$$

$$= -\sum_{kk'} \frac{n_k - n_{k'}}{E_k - E_{k'} + \hbar\omega + i\delta} \times \langle\psi_k|\, e^{-i\vec{q}\cdot\vec{r}}\,|\psi_{k'}\rangle\langle\psi_{k'}|\, e^{i\vec{q}\cdot\vec{r}}\,|\psi_k\rangle\ . \tag{3}$$

Here $E_k$ is the Bloch energy of the state $k$ with Bloch function $\psi_k$ and occupation number $n_k$; $k$ includes both the band index and the wave vector $\vec{k}$ which is restricted to the first Brillouin zone. The oscillator-strength matrix element

$$M_{kk'}(\vec{q}) = \langle\psi_k|\, e^{-i\vec{q}\cdot\vec{r}}\,|\psi_{k'}\rangle\ , \tag{4}$$

imposes the restriction $\vec{k}' = \vec{k} + \vec{q} + \vec{G}$, where $\vec{G}$ is a reciprocal-lattice vector; $\omega$ denotes the frequency of the external field, and $\chi(\vec{q},\omega)$ is the bare susceptibility of the solid, i.e., the effects due to local fields are not included. The zeros of $\epsilon_1(\vec{q},\omega) = \mathrm{Re}[\epsilon(\vec{q},\omega)]$ determine the plasmon dispersion relation and $\epsilon_2(\vec{q},\omega) = \mathrm{Im}[\epsilon(\vec{q},\omega)]$ is related to many properties including the dynamic form factor $S(\vec{q},\omega)$, the optical conductivity, and the optical reflectivity.[3]

The static response function $\chi(\vec{q})$, i.e., the response function for $\omega = 0$ is itself of very great interest because of its possible role in causing electronically driven instabilities which are manifested as spin-density waves, charge-density waves, or in structural phase transformations. From Eq. (3) we can write down the expression for $\chi(\vec{q})$:

$$\chi(\vec{q}) = \chi(\vec{q},\omega=0) = -\sum_{kk'} \frac{n_k - n_{k'}}{E_k - E_{k'}} |M_{kk'}(\vec{q})|^2 = -2\sum_{kk'} \frac{n_k(1-n_{k'})}{E_k - E_{k'}} |M_{kk'}(\vec{q})|^2\ . \tag{5}$$

It has been argued that due to the "nesting" features, i.e., the existence of flat and parallel areas of the Fermi surface, the denominator in Eq. (5), will tend to be vanishingly small, giving rise to a large peak in $\chi(\vec{q})$ at the nesting wave vector. Such a large peak in $\chi(\vec{q})$ coupled with exchange enhancement effects in, for instance, paramagnetic chromium,[4,5] has been thought to be the main reason for driving the paramagnetic phase unstable with respect to an antiferromagnetic phase, and has since been used by a number of workers to account for various other instabilities related to Fermi-surface geometry. The occurrence of anomalies in phonon spectra of metals has also been related in a similar way to

the sharp features in $\chi(\vec{q})$. But before one can have faith in the relationship between nesting features of the Fermi surface and observed instabilities, we must note that while nesting features are important, the effect of the oscillator-strength matrix elements, $M_{kk'}(\vec{q})$ has been almost totally ignored in favor of the energy denominator part of $\chi(\vec{q})$, i.e., the oscillator-strength matrix elements have been assumed constant and attention has been focused just on $\bar{\chi}(\vec{q})$, where

$$\bar{\chi}(\vec{q}) = 2\sum_{kk'} \frac{n_k(1-n_{k'})}{E_{k'}-E_k} \quad . \tag{6}$$

The justification for such an approximation has usually been based on the beliefs (i) that the oscillator-strength matrix elements $M_{kk'}(\vec{q})$ depend very weakly on $k$, and they are smoothly and slowly varying functions of $\vec{q}$ only; and (ii) that the wave vector where instability occurs, i.e., the position of the peak in the generalized susceptibility function $\chi(\vec{q})$, will be determined largely from the nesting features of the Fermi surface. Calculations of $\chi(\vec{q})$ for[1] Cr and[2] Nb including matrix elements have shown that these approximations are, at best, very crude and that the effect of matrix elements is rather dramatic. It is clear from Eq. (3) that in the $\vec{q}\to 0$ limit, the interband matrix elements vanish while the intraband matrix elements tend to unity resulting in $\chi(\vec{q})$ tending to the density of states of the Fermi level. Since the matrix elements are ignored in Eq. (6), both intraband and interband transitions contribute to $\bar{\chi}(\vec{q})$, and hence $\bar{\chi}(\vec{q})$ will deviate considerably from the correct value at $\vec{q}=0$. In fact, it was found that in the case of Cr, the value of $\bar{\chi}(\vec{q})$ was almost 20 times $\chi(\vec{q})$. In the large-$\vec{q}$ limit, on the other hand, the intraband matrix elements will be rather small, and it is really the interband contributions which will dominate. The behavior of the interband matrix elements in this limit cannot be easily simulated without an actual calculation using Bloch functions from an energy-band calculation. In general, both intraband and interband matrix elements in transition metals will have quite complicated behavior and will be strongly dependent both on the initial and final Bloch states $\vec{k}$ and $\vec{k}'$ ($\vec{k}'=\vec{k}+\vec{q}+\vec{G}$), and not just on $\vec{q}$. The strong $k$ and $\vec{q}$ dependence will manifest itself even more in the region where the bands are strongly hybridized.

Accurate calculations of $\chi(\vec{q})$ are now possible since we have confidence in the accuracy of the essential ingredients entering Eq. (5), namely, the electronic energy bands and wave functions derived from, for instance, augmented-plane-wave (APW) calculations. The Brillouin-zone integration techniques—a very important ingredient for an accurate determination of $\chi(\vec{q})$—have been sufficiently refined and speeded up during the last year. In particular, the analytic tetrahedron linear energy method[6] has been shown to be simple to use and to be capable of giving results which are accurate to within 1% for an idealized system where analytic results are available for comparison.

In this paper we present results for the case of scandium metal, and examine in detail the importance of including the matrix elements in the calculation of $\chi(\vec{q})$. Our motivation to study the transition metal scandium arises from the fact that Sc and Y have many properties which very closely resemble those of the heavy-rare-earth metals. Sc itself is nonmagnetic, but its alloys with magnetic rare earths do show magnetic structure with the magnetic wave vector $\vec{q}_m=(0,0,0.56\pi/c)$.[7] The phonon spectra of Sc, available from the neutron scattering work of Wakabayashi, Sinha, and Spedding[8] show an anomaly in the longitudinal-acoustic (LA) branch at a wave vector $\vec{q}=(0,0,0.54\pi/c)$. Both the wave vector for the magnetic ordering and the wave vector for the phonon anomaly agree very well with the nesting feature in the $c$ direction found in our calculation[6] of the Fermi surface of Sc, and by Fleming and Loucks[9] in an earlier calculation. Since the nesting feature in the Fermi surface of scandium is found in the $c$ direction, and since we are mainly interested in the influence of matrix elements on the nesting-related peaks in the generalized susceptibility function, we have performed the calculation of $\chi(\vec{q})$ for $\vec{q}$ only in the $c$ direction. Furthermore, we have included only the third and the fourth bands in our calculation since only these two bands determine the Fermi surface. For the Brillouin-zone integration we employ the accurate tetrahedron method of Rath and Freeman,[6] mentioned earlier. The electronic band structure and Fermi surface of Sc are discussed in Sec. II. Comparison is made between the single- and double-zone schemes in Sec. III where our results for $\chi(\vec{q})$ in the constant-matrix-element approximation are presented. The calculation of oscillator-strength matrix elements is described in Sec. IV, which presents our results for $\chi(\vec{q})$ obtained with the inclusion of matrix elements. Finally, the effects of local-field corrections are discussed, and the results of a crude calculation are presented.

## II. ELECTRONIC STRUCTURE OF SCANDIUM

The starting point for the calculation of the generalized susceptibility function $\chi(\vec{q})$ of a solid is the determination of its electronic band structure. In the present work we have calculated the energy bands and wave functions of scandium metal by means of the APW method.[10] The neutral atom charge densities for the atomic configuration

$3d^24s^1$ obtained from the Herman-Skillman Hartree-Fock-Slater self-consistent atomic calculations were used to construct the crystal potential in the warped-muffin-tin approximation, i.e., the crystal potential in the interstitial region was not assumed to be constant. The contribution of exchange was included using Slater's $\rho^{1/3}$ approximation with $\alpha = 1$. Instead of choosing a different basis set for each point in the Brillouin zone, a universal basis set of 49 reciprocal-lattice vectors was used in the expansion of the wave functions. The lattice constants, $a = 6.23912$ a.u. and $c = 9.93164$ a.u., were taken from the recent low-temperature work of Mueller.[11] We chose the radius of the muffin-tin sphere as $R_{MT} = 2.9872$ a.u., which is close to the maximum allowable radius 3.0674 a.u. of half the nearest-neighbor distance. With our basis set, the energy eigenvalues were converged to within 1 mRy at high-symmetry points. These results are in agreement with the earlier nonrelativistic results of Fleming and Loucks[9] and Rath and Freeman[6] and the relativistic results of Das *et al.*[12] except for some small differences arising from the different atomic configuration and/or lattice constants used.

The hexagonal-close-packed structure has two atoms in the unit cell. The structure factor and the Fourier coefficient of the potential vanish for reciprocal-lattice vectors which have their $z$ component an odd multiple of $2\pi/c$. The Brillouin-zone-boundary planes normal to the hexagonal axis are planes containing a time-reversal degeneracy. This causes the energy eigenvalues in the $AHL$ plane to be degenerate in pairs of two; e.g., first and second band, third and fourth band, etc., are degenerate in the $AHL$ plane. This degeneracy is lifted (except along the $AL$ line) by the spin-orbit coupling, but since scandium is a light metal, such effects are unimportant and we shall not consider them in the present work. As a consequence of this degeneracy in the $AHL$ plane, one can visualize, for instance, the first and second band as one continuous band by unfolding the second band into the extended zone $A$-$\Gamma$ as is shown schematically in Fig. 1. This is equivalent to doubling the period in the $c$ direction; that is, to using a Brillouin zone double its original size in the $c$ direction.

The decision as to the use of the single or double zone depends on the problem at hand. For example, the Fermi surface may be quite conveniently plotted in this so-called double-zone scheme without any approximation. But the use of the double-zone scheme implies that direct optical transitions from, for instance, $a$ to $b'$ (see Fig. 1) do not occur because they do not conserve crystal momentum. However, these transitions are in fact equivalent to the $a$ to $b$ transitions which do occur.

The Fermi surface of scandium determined in the double-zone scheme is basically the same as found earlier by Fleming and Loucks.[9] The Fermi level was calculated using the tetrahedron method,[6] and was found to be 0.455 Ry (relative to the constant potential in the interstitial region $V_0 = -1.04550$ Ry). The density of states at the Fermi energy $N(E_F)$ is 30 states/Ry atom, in good agreement with other calculations.[6,9,12]

## III. CALCULATION OF $\bar{\chi}(\vec{q})$

The structure in the generalized susceptibility function is very sensitive to the Brillouin-zone integration procedure. In the present work we have used the analytic tetrahedron linear energy method (henceforth referred to as the tetrahedron method) developed by Rath and Freeman[6] for the calculation of the generalized susceptibility function with both constant matrix elements $\bar{\chi}(\vec{q})$ and with APW matrix elements $\chi(\vec{q})$. Rath and Freeman have discussed in detail the tetrahedron method, its accuracy and advantages over other existing methods, and have also used it to calculate $\bar{\chi}(\vec{q})$ for Sc, and of some model systems.[6] In the tetrahedron method, the whole Brillouin zone is divided into microzones which are tetrahedrons inside which the variation of energy is assumed linear. If one assumes that inside each tetrahedron the matrix elements are constant, then the contribution to $\chi(\vec{q})$ is obtained as an analytic expression which depends only on the energies at the corners of the tetrahedron. The method is accurate and simple to use.

The calculation of $\bar{\chi}(\vec{q})$ for Sc has already been described elsewhere.[6] These authors performed the calculation in the double-zone scheme as discussed in Sec. II using only third and fourth bands which determine the Fermi surface. However, since the mesh used in our calculation is slightly different, it was thought worthwhile to repeat their

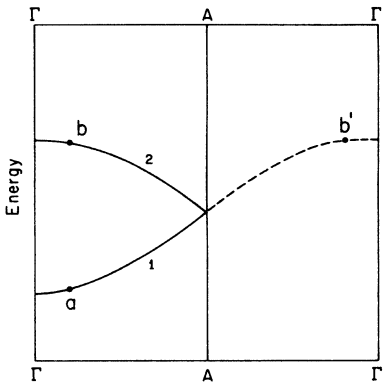


FIG. 1. Double-zone scheme for the hexagonal-close-packed lattice.

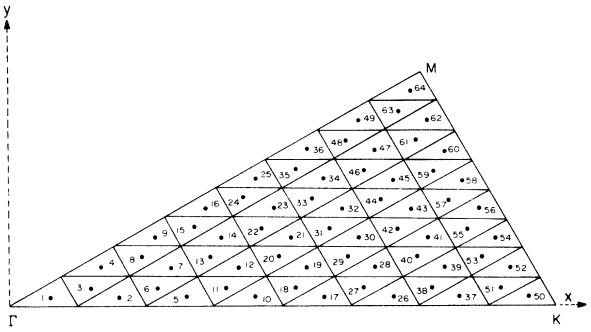


FIG. 2. Mesh of points (projected in the basal plane) used in the calculation of $\bar{\chi}(\vec{q})$ and $\chi(\vec{q})$. Dots indicate the centers of the triangular prisms where the oscillator-strength matrix elements are calculated.

calculation to facilitate a more meaningful comparison with $\chi(\vec{q})$. The grid of points used in our calculation is shown for an irreducible basal plane section in Fig. 2, with the $\Gamma K$ and $\Gamma M$ distance each divided into eight parts. Since $\Gamma A$ distances were divided into 10 parts, there are 11 such planes in the irreducible Brillouin zone, and each plane contains 64 triangles of equal area. Thus, there are a total of 640 triangular prisms in each $\frac{1}{24}$th of the irreducible Brillouin zone, or equivalently, 15 360 triangular prisms in the entire first Brillouin zone (BZ); each prism accomodates three tetrahedrons.

It has been usual practice to calculate $\bar{\chi}(\vec{q})$ in the double-zone scheme. From our discussion in Sec. II (cf. Fig. 1) about the double-zone scheme, it is clear that the effect of treating the two bands of the single-zone scheme in the double-zone scheme is to allow only the intraband couplings if $(\vec{k}+\vec{q})_z$ remains in the first BZ, and only the interband couplings if $(\vec{k}+\vec{q})_z$ is outside the first BZ *and* a reciprocal-lattice vector $2\pi/c$ is required to bring it back to the first BZ. Furthermore, if the allowed matrix elements are assumed constant (which is usually the case) then the matrix elements are such that

$$M_{\vec{k}_i,(\vec{k}+\vec{q})_j} = \begin{cases} \delta_{ij} & \text{if } |k_z+q_z| \le \pi/c \\ 1-\delta_{ij} & \text{if } |k_z+q_z| > \pi/c\ , \end{cases} \tag{7}$$

where $i$ and $j$ are the band indices in the single-zone scheme. [In this connection we should mention that since the actual matrix elements $M_{kk'}(\vec{q})$ are step functions (i.e., 1 or 0 depending on whether $\vec{k}$ is equal or not equal to $\vec{k}+\vec{q}$) for the free-electron-gas case, their effect is included explicitly if one uses the *extended-zone scheme*. Thus, Eq. (6) will yield the Lindhard function only in the *extended*-zone scheme. In the reduced-zone scheme the use of constant matrix elements will not yield the usual Lindhard result unless matrix elements (1 or 0) are included.]

The calculations reported so far for the hexagonal-close-packed metals Sc, Y, and the heavy rare earths[13,14] have been based on the two-band model (single-zone scheme) where two bands, the third and the fourth, which are responsible for the Fermi-surface features of these metals, have been used in calculating $\bar{\chi}(\vec{q})$. It is easy to see that in this two-band model, use of the double-zone scheme, or alternatively the use of Eq. (7) for the matrix elements, is a simple extension of the free-electron case where the matrix elements are implicitly included in the extended-zone scheme. As we shall see in Sec. V, considerable deviations occur for transition metals from the matrix elements given in Eq. (7), particularly in the region where there is strong mixing between the bands.

In order to maintain a close similarity between the calculations of both $\bar{\chi}(\vec{q})$ and $\chi(\vec{q})$, we made use of Eq. (7) for the step-function matrix elements in the double-zone scheme in two ways. We did not use the double-zone scheme for $\bar{\chi}(\vec{q})$ by unfolding the fourth band into the extended zone. In the first case matrix elements pertinent to Eq. (7) which are 1 or 0 were evaluated at the *center of each tetrahedron*. In the second case they were evaluated at the *center of each triangular prism* (which accommodates three tetrahedrons). We found that the results from these two calculations were almost identical. They also agree well with the earlier calculations of Rath and Freeman. We show in Fig. 3 our $\bar{\chi}(\vec{q})$ calculated along $\Gamma A$ using Eq. (7) either at the center of the tetrahedrons or at the center of the triangular prisms. It is gratifying to note that it is possible to ignore the variation of the matrix elements over a small volume without affecting the accuracy of the results. This is an important consideration when one includes the matrix elements calculated with actual Bloch functions, as is done with APW wave functions in Sec. IV. It is clear that by using the APW matrix elements at the center of each triangular prism rather than at the center of each tetrahedron, and assuming them constant throughout the microzone, considerable saving in machine time as well as programming effort can be achieved.

From Fig. 3 we note that there are two sharp peaks in $\bar{\chi}(\vec{q})$—one at approximately $\vec{q}=0.60\pi/c$ and another at approximately $1.40\pi/c$. The first peak position agrees very well with both the magnetic wave vector observed in scandium–rare-earth alloys and the $\vec{q}$ vector for the phonon anomaly. It also agrees very well with the nesting wave vector found in the Fermi surface which connects the third-band hole surface to the fourth-band electron surface. To understand the origin of the peaks in

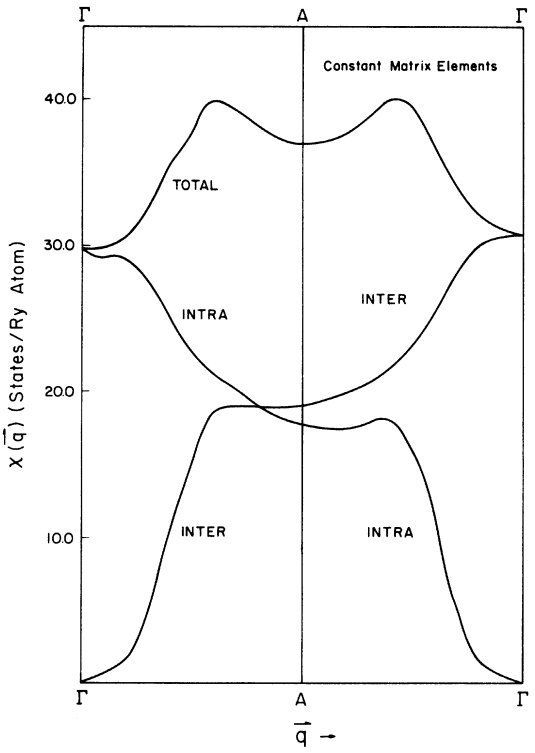


FIG. 3. Generalized susceptibility function $\bar{\chi}(\vec{q})$ of Sc metal in the double-zone scheme (in the constant matrix elements approximation) for $\vec{q}$ along $\Gamma A$.

$\bar{\chi}(\vec{q})$, we have separated the intraband and interband contributions, and plotted them in Fig. 3. Quite surprisingly, there is no sharp peak in the interband part as implied by the "nesting" hypothesis, although there is certainly a shoulder around $\vec{q}=0.60\pi/c$. The peak at this wave vector in fact arises from the fact that with increasing $\vec{q}$ the interband part of $\bar{\chi}(\vec{q})$ is rising faster than the intraband part is dropping, until the interband part becomes constant in the region of the peak and the intraband part shows a plateau and starts dropping again. A similar behavior around $\vec{q}=1.40\pi/c$ results in a second sharp peak in $\bar{\chi}(\vec{q})$. The origin of this behavior of the intraband and interband parts of $\bar{\chi}(\vec{q})$ is probably the same as that which gives sharp peaks (or critical points) in the joint density of states. Clearly Fermi-surface nestings do help in the formation of peaks in $\bar{\chi}(\vec{q})$, but they may not be the dominant cause, as has been found in the present case.

## IV. CALCULATION OF $\chi(\vec{q})$

### A. Calculation of the oscillator-strength matrix elements

In order to calculate $\chi(\vec{q})$, we need to obtain the expression for the oscillator strength matrix elements $M_{kk'}(\vec{q})$ defined in Eq. (4). In the APW method[10] the Bloch function $\psi_k(\vec{r})$ is expanded in the APW's in the following manner:

$$\psi_k(\vec{r})=\frac{1}{\sqrt{\Omega}}\sum_{\vec{g}} a_{\vec{g}}(k)\Phi_{\vec{g}}(k,\vec{r})\,, \tag{8}$$

where $\Omega$ is the crystal volume, $a_{\vec{g}}(k)$ is the coefficient of expansion determined variationally from the APW secular equation, $\vec{g}$ is the reciprocal-lattice vector used in the expansion, and $\Phi_{\vec{g}}(k,\vec{r})$ is an APW defined as

$$\Phi_{\vec{g}}(k,\vec{r})=e^{i(\vec{k}+\vec{g})\cdot\vec{r}}\,, \tag{9}$$

for $\vec{r}$ in the interstitial region, and

$$\Phi_{\vec{g}}(k,\vec{r})=4\pi e^{i(\vec{k}+\vec{g})\cdot(\vec{R}_n+\vec{R}_\nu)} \times\sum_{lm} i^l j_l(|\vec{k}+\vec{g}|R)\,Y^*_{lm}\left(\frac{\vec{k}+\vec{g}}{|\vec{k}+\vec{g}|}\right)Y_{lm}(\hat{\rho})R_l(k,\rho)\,, \tag{10}$$

inside the muffin-tin spheres. Here $R$ is the radius of the muffin-tin sphere around each scandium nucleus, and the distance $\vec{r}$ from the origin has been expressed as

$$\vec{r}=\vec{R}_n+\vec{R}_\nu+\vec{\rho}\,, \tag{11}$$

where $\vec{R}_n$ is the translation vector and $\vec{R}_\nu$ is the position of the $\nu$th basis atom inside the unit cell. The vector $\vec{\rho}$ is now measured from the center of the muffin-tin sphere. $R_l(k,\rho)$ denotes the radial wave function which, of course, depends only on the band energy and not the Bloch wave vector $\vec{k}$. In Eq. (10) we have normalized $R_l(k,\rho)$ so that it has the value unity at the muffin-tin boundary. All other symbols have their usual meaning.[10] Inside the muffin-tin spheres we may combine Eqs. (8) and (10), and rewrite the Bloch function as

$$\psi_k(\vec{r})=\frac{1}{\sqrt{\Omega}}\sum_{\vec{g}} a_{\vec{g}}(k)\,4\pi e^{i(\vec{k}+\vec{g})\cdot(\vec{R}_n+\vec{R}_\nu)}\sum_{lm} i^l j_l(|\vec{k}+\vec{g}|R)\,Y^*_{lm}\left(\frac{\vec{k}+\vec{g}}{|\vec{k}+\vec{g}|}\right)Y_{lm}(\hat{\rho})R_l(k,\rho)$$
$$=\frac{e^{i\vec{k}\cdot(\vec{R}_n+\vec{R}_\nu)}}{\sqrt{\Omega}}\sum_{lm} i^l A^\nu_{lm}(k)\,Y_{lm}(\hat{\rho})R_l(k,\rho), \tag{12}$$

where

$$A^\nu_{lm}(k)=4\pi\sum_{\vec{g}} e^{i\vec{g}\cdot\vec{R}_\nu}\,j_l(|\vec{k}+\vec{g}|R)\,Y^*_{lm}\left(\frac{\vec{k}+\vec{g}}{|\vec{k}+\vec{g}|}\right)a_{\vec{g}}(k)\,. \tag{13}$$

The APW wave function inside the muffin-tin spheres in the form of Eq. (12) was also similarly expressed by Gupta and Sinha.[1] This form not only simplifies considerably the evaluation of the oscillator-strength matrix elements but is also intuitively appealing because of its close resemblance to the Korringa-Kohn-Rostoker form. The expression for the oscillator-strength matrix elements $M_{kk'}(\vec{q})$ can then be written

$$M_{kk'}(\vec{q}) = \langle \psi_k | e^{-i\vec{q}\cdot\vec{r}} | \psi_{k'} \rangle = \sum_{\vec{g}\,\vec{g}'} a^*_{\vec{g}}(k) a_{\vec{g}'}(k') \left( \delta_{\vec{K},0} - \frac{2V_0}{\Omega_0} G(KR) S(\vec{K}) \right) + M^i_{kk'}(\vec{q}) , \tag{14}$$

where $\vec{K} = \vec{k}' + \vec{g}' - \vec{k} - \vec{g} - \vec{q}$ is a reciprocal-lattice vector, $S(\vec{K})$ is the structure factor $S(\vec{K}) = \frac{1}{2}\sum_\nu e^{i\vec{K}\cdot\vec{R}_\nu}$, $V_0$ and $\Omega_0$ are the volumes of a muffin-tim sphere and the unit cell, respectively, and the function $G(KR)$ is defined as

$$G(x) = 3(\sin x - x\cos x)/x^3 . \tag{15}$$

$M^i_{kk'}(\vec{q})$ is the contribution to $M_{kk'}(\vec{q})$ due to the part inside the muffin-tin spheres, and is given by

$$M^i_{kk'}(\vec{q}) = \frac{4\pi}{\Omega_0} \sum_\nu e^{i\vec{G}\cdot\vec{R}_\nu} \sum_{lm} \sum_{l'm'} \sum_{l''m''} i^{-l+l'-l''} A^{*\nu}_{lm}(k) A^{\nu}_{l'm'}(k') Y_{l''m''}(\hat{q}) T(ll'l'', kk'q) G(lm\,l'm'l''m'') . \tag{16}$$

Here $\vec{G} = \vec{k}' - \vec{k} - \vec{q}$ is a reciprocal-lattice vector which brings $\vec{k} + \vec{q}$ back to the first Brillouin zone, and

$$T(ll'l'', kk'q) = \int_0^R j_{l''}(q\rho) R_l(k,\rho) R_{l'}(k',\rho) \rho^2 d\rho , \tag{17}$$

$$G(lm\,l'm'l''m'') = \int Y^*_{lm}(\hat{\rho}) Y_{l'm'}(\hat{\rho}) Y^*_{l''m''}(\hat{\rho}) d\hat{\rho} . \tag{18}$$

$G(lm\,l'm'\,l''m'')$ are, of course, related to the Clebsch-Gordan coefficients.[15] Clearly the expression for the matrix elements is quite cumbersome and time consuming on a machine. Because one needs to evaluate a very large number of these matrix elements in order to compute $\chi(\vec{q})$, one needs to evaluate them as economically as possible. In our calculation, we restricted the maximum value of $l$ and $l'$ to 2 (and hence $l''$ to 4) and renormalized the wave functions accordingly. It was observed, however, that the higher-$l$ components did not contribute significantly to the wave functions in the muffin-tin region—a fact expected intuitively from the success of the Korringa-Kohn-Rostoker method.

It was noted in Sec. III that $\bar{\chi}(\vec{q})$ was practically unchanged whether we evaluated the step-function matrix elements of Eq. (7) at the center of each tetrahedron, or at the center of each triangular prism comprising three tetrahedrons, assuming them constant throughout the microzone. We have made use of this result to reduce the number of matrix elements entering our calculation of $\chi(\vec{q})$. As stated before, we used only third and fourth bands in our calculation and for each band, Bloch functions were calculated at the center of each triangular prism. This amounts to calculating and using 1280 wave functions in the irreducible part of the Brillouin zone. The matrix elements from Eq. (14) are evaluated at the center of each of these prisms. (cf. Fig. 2 which shows the projections of the centers of the prisms onto the basal plane.) Since in our calculation, $\vec{q}$ is restricted to the $c$ direction and since the values of $\vec{q}$ we chose are commensurate with the mesh points in the $c$ direction, $\vec{k}+\vec{q}$ reduced to the first Brillouin zone falls in the same chain of prisms as does $\vec{k}$. Thus the programming and calculational effort is reduced considerably.

In Sec. II we discussed briefly the double-zone scheme (DZS). It was stated that in the two band model the DZS allows only the intraband couplings if $(\vec{k}+\vec{q})_z$ lies in the first Brillouin zone, and only the interband couplings if $(\vec{k}+\vec{q})_z$ falls outside the first BZ. It is clear that in general both intraband and interband contributions will be permitted and the use of the DZS introduces approximations. Furthermore, the matrix elements for the allowed transitions will, in general, not be constant. The validity of these approximations can only be checked by an actual calculation of the matrix elements. In what follows we shall present plots of matrix elements for some $\vec{k}$ and $\vec{q}$ points. The dominant matrix elements are, of course, those allowed in the DZS. For this reason and for the sake of clarity we plot the matrix elements as if the fourth band was unfolded into the extended $A\Gamma$ zone. The couplings allowed in this one band or the double-zone picture will be labeled as "DZS," and the extra couplings not permitted in the DZS will be referred to as the deviations from the DZS.

In Fig. 4 we have plotted the matrix elements as a function of $\vec{q}$. The initial state vector $\vec{k}$ for these matrix elements has been fixed at a point very close to $\Gamma$ (i.e., point "1" in Fig. 2 with its $z$ component equal to $0.05\pi/c$). The vector $\vec{q}$ has been varied from 0 to $2\pi/c$ in the $c$ direction, with both positive and negative $\vec{q}$ values. The left side of Fig. 4 shows the results for $-\vec{q}$, and the right

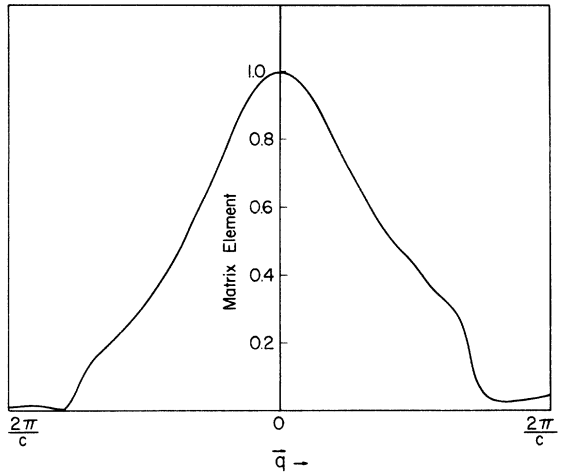


FIG. 4. Matrix elements $M_{kk'}(\vec{q})$ for the $k$ point marked "1" in Fig. 2 with $k_z = 0.05(\pi/c)$. The left side shows the matrix elements for $-\vec{q}$ and the right $+\vec{q}$.

side for $+\vec{q}$. The final state vector $\vec{k}+\vec{q}$, of course, varies in the $c$ direction with its $x$ and $y$ coordinates again given by the point marked "1" in Fig. 2. From Fig. 4 we see that although the matrix elements are varying more or less smoothly as a function of $\vec{q}$, they are *not* slowly varying functions of $\vec{q}$. Needless to say, except in the small-$\vec{q}$ regime, they are far from unity. Another interesting feature we note is the asymmetry, i.e., the matrix elements for forward scattering $+\vec{q}$ are not equal to the ones for backward scattering $-\vec{q}$. In Fig. 5 we show the energy bands which are involved in determining the matrix elements shown in Fig. 4. We see that there is considerable interaction between the fourth and fifth bands,

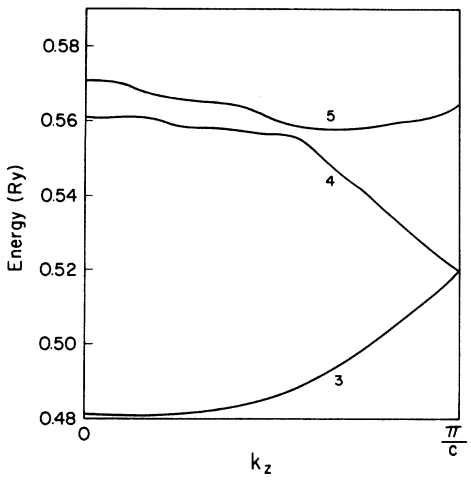


FIG. 5. Energy bands which are involved in the determination of the matrix elements shown in Fig. 4.

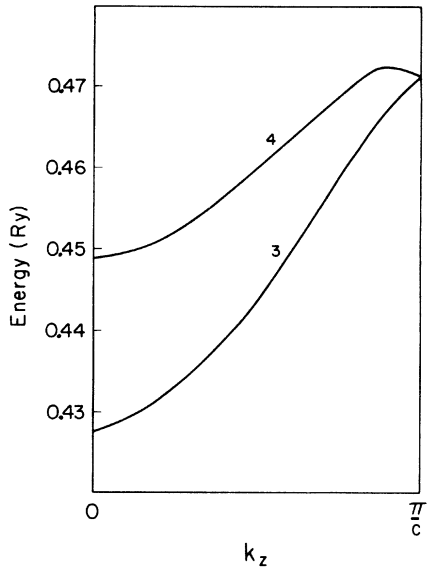


FIG. 6. Energy bands for the $k$ point marked "29" in Fig. 2 with $k_z$ varying from 0 to $\pi/c$.

and this is reflected in the matrix elements in the large-$\vec{q}$ limit as seen in Fig. 4. We recall that in the DZS, it is only in the large-$\vec{q}$ limit that the part of the fourth band which is strongly hybridized with the fifth band enters into the matrix-element calculation. Incidentally, for these bands there is very little deviation (~ 2%) from the DZS and it has therefore not been shown in Fig. 4. Looking at the bands in Fig. 5, this is expected since the third and the fourth bands themselves are well separated. That this is not always the case, and considerable deviations occur from the DZS, can be seen if we choose the points far from the origin.

In Fig. 6 we show the energy dispersion in the $c$ direction for the third and fourth bands for the point marked "29" in Fig. 2. As we see, the energy separation between these two bands is rather small; its maximum separation is only 0.02 Ry. This behavior results in matrix elements which are strongly $\vec{k}$ and $\vec{q}$ dependent and show considerable asymmetry for $+\vec{q}$ and $-\vec{q}$. Since the Fermi energy is 0.455 Ry, and since part of the fourth band is below the Fermi level, transitions originating from the occupied portion of both third and fourth bands will contribute to the $\chi(\vec{q})$. Figure 7 shows the matrix elements resulting from transitions from the third to the fourth band plotted as a function of $\vec{k}_z$, the $z$ component of the initial state vector; for each curve the $\vec{q}$ vector is fixed to a value marked on the curve. Similarly, Fig. 8 shows the matrix elements for transitions from the fourth to the third band. In both cases, we find that except for small-$\vec{q}$ values,

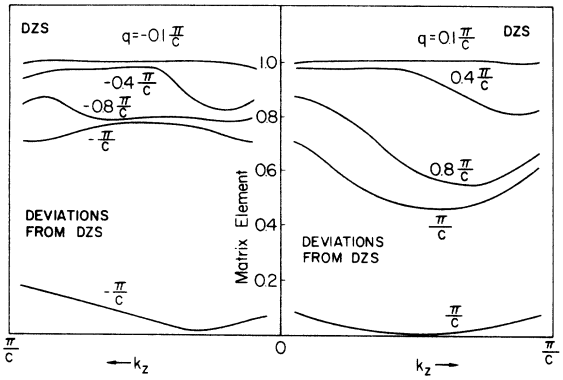


FIG. 7. Matrix elements $M_{kk'}(\vec{q})$ as a function of $k_z$ (the point marked "29" in Fig. 2 determines the $k_x$ and $k_y$ components) for different values of $\vec{q}$ along the $c$ direction shown on each curve. The upper curves marked DZS show the couplings which are allowed in the double-zone scheme. The lower curve shows the couplings for $\vec{q} = \pm \pi/c$ which are forbidden by the concept of the double-zone scheme. All the matrix elements shown above arise from transitions from the third band to the third and fourth bands.

the matrix elements are not at all constant. We note that the matrix elements for a fixed-$\vec{q}$ value are strongly dependent on the vector $\vec{k}$, with a dependence which becomes increasingly prominent with increasing values of $\vec{q}$. We note also the considerable deviation from the DZS, as is shown in the curves at the bottom of the figures. As with the $\vec{k}$ dependence, the deviation from the DZS increases with increasing values of $\vec{q}$. Finally, the results show a very substantial asymmetry for positive and negative values of $\vec{q}$.

### B. Results for $\chi(\vec{q})$

Following the procedure discussed above for calculating the oscillator-strength matrix elements, and using the grid of points shown in Fig. 2, we calculate $\chi(\vec{q})$ from Eq. (5). As with $\bar{\chi}(\vec{q})$, the calculation was performed for $\vec{q}$ varying from $\vec{q}=0$ to $\vec{q}=2\pi/c$ in the $c$ direction in intervals of $0.10\pi/c$. We show in Fig. 9 the intraband and interband contributions to $\chi(\vec{q})$, and their counterparts from $\bar{\chi}(\vec{q})$ for comparison. We note that $\chi_{\text{intra}}$ does not differ substantially from $\bar{\chi}_{\text{intra}}$ at low-$\vec{q}$ vectors but as $\vec{q}$ increases, the discrepancy increases and reaches a maximum at $\vec{q} \approx 1.4\pi/c$ where $\bar{\chi}_{\text{intra}}$ is more than two times $\chi_{\text{intra}}$. For $\vec{q} > 1.4\pi/c$ both $\chi_{\text{intra}}$ and $\bar{\chi}_{\text{intra}}$ begin to fall off rapidly and are vanishingly small at $\vec{q} \approx 2\pi/c$. The broad peak in $\bar{\chi}_{\text{intra}}$ at $\vec{q} \approx 1.4\pi/c$ still shows up in $\chi_{\text{intra}}$ but with reduced magnitude.

The most conspicuous change, however, is found in the interband part of the susceptibility. Both $\chi_{\text{inter}}$ and $\bar{\chi}_{\text{inter}}$ start from zero values at $\vec{q}=0$, and the difference between them is small for small values of $\vec{q}$. This similarity, however, ends at $\vec{q} \approx 0.35\pi/c$. Although the $\chi_{\text{inter}}$ keeps rising until it shows a peak at $\vec{q} = 0.60\pi/c$, $\bar{\chi}_{\text{inter}}$ rises much faster. Thus, whereas $\chi_{\text{inter}}$ at $\vec{q} = 2\pi/c$ is rather small, $\bar{\chi}_{\text{inter}}$ is larger than ever because the DZS, in conjunction with the step-function matrix elements, permits only the inter-

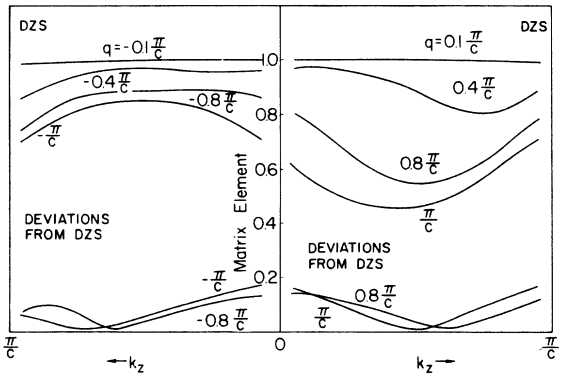


FIG. 8. Same as Fig. 7 except that these matrix elements arise from transitions from the fourth band to the fourth band and the third band.

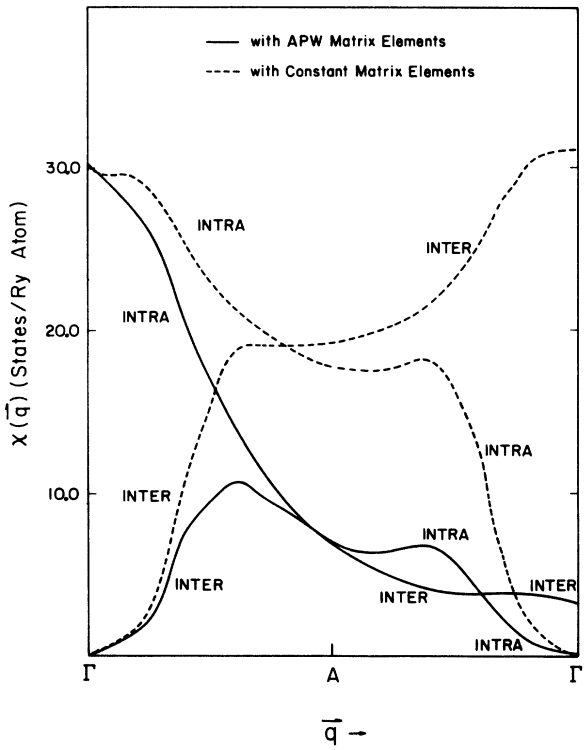


FIG. 9. Intraband and interband parts of the generalized susceptibility function. The solid curves include the APW matrix elements and the dashed curves show the counterparts from $\bar{\chi}(\vec{q})$.

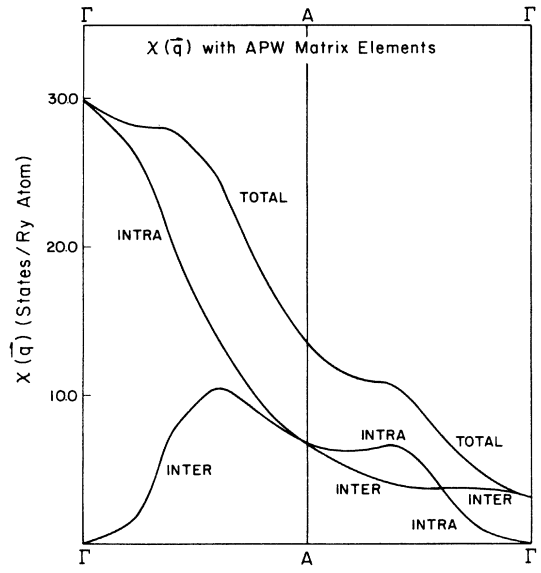


FIG. 10. Generalized susceptibility function $\chi(\vec{q})$ including APW matrix elements.

band contribution in $\bar{\chi}_{\text{inter}}$, whereas $\chi_{\text{inter}}$ is suppressed by the inclusion of the oscillator-strength matrix elements. An interesting feature in $\chi_{\text{inter}}$, however, is that the broad shoulder in $\bar{\chi}_{\text{inter}}$ at $\vec{q}=0.60\pi/c$ has been sharply focused into a small peak. [We note in this respect the interesting result of Cooke *et al.*[2] that the inclusion of matrix elements brought out structure in the $\chi(\vec{q})$ of Nb which was not found in $\bar{\chi}(\vec{q})$.]

The total $\chi(\vec{q})$ is shown in Fig. 10. We note that the peak in $\chi_{\text{inter}}$ at $\vec{q}=0.60\pi/c$ is not present in $\chi(\vec{q})$. The intraband contribution has fallen off so much at this wave vector that the total $\chi$ is unable to sustain the peak found in interband part. We find that the over-all shape of $\chi(\vec{q})$ curve is totally different from that of $\bar{\chi}(\vec{q})$, and the influence of the oscillator-strength matrix elements has been rather drastic.

### C. Effect of local-field corrections on the phonon anomaly and magnetic ordering

Since the inclusion of the matrix elements results in the generalized susceptibility function not showing a peak at a wave vector where the phonon anomaly is observed, the question remains as to how can one explain the observed phonon anomaly. It is now recognized that the local-field corrections play an important role in determining the phonon spectrum of transition metals and insulators.[16,17] The off-diagonal elements of the dielectric matrix $\epsilon(\vec{Q},\vec{Q}')$

$$\epsilon(\vec{Q},\vec{Q}') = \delta_{\vec{Q}\vec{Q}'} + v(\vec{Q})\chi(\vec{Q},\vec{Q}') \ , \tag{19}$$

where

$$\chi(\vec{Q},\vec{Q}') = \sum_{kk'} \frac{n_k - n_{k'}}{E_{k'} - E_k} \langle \psi_k | e^{-i\vec{Q}\cdot\vec{r}} | \psi_{k'} \rangle \times \langle \psi_{k'} | e^{i\vec{Q}'\cdot\vec{r}} | \psi_k \rangle \tag{20}$$

are not insignificant in comparison to the diagonal matrix elements. Evidently, such off-diagonal terms will have an important effect on the diagonal elements of the inverse dielectric matrix $\epsilon^{-1}(\vec{Q},\vec{Q}')$ which is what really enters into the calculation of phonon spectra. It is not clear whether the local-field corrections of this type can simulate structure or a peak in $\epsilon^{-1}(\vec{Q},\vec{Q}')$ at the observed wave vector. In any case, $\epsilon^{-1}(\vec{Q},\vec{Q}')$ is only one of the two necessary ingredients entering the calculation of phonon spectrum, the other being the electron-ion interaction; the combination of the two gives rise to phonon anomalies. Evidently, the structure in $\chi(\vec{Q})$ or $\epsilon^{-1}(\vec{Q},\vec{Q}')$ may be helpful in giving rise to phonon anomalies, but it is by no means essential. This view is supported by the recent work of Sinha and Harmon[18] on Nb metal and NbC where it has been found that the phonon anomalies may appear without any peaks in $\chi(\vec{Q})$.

As mentioned previously, Sc metal is nonmagnetic. When alloyed with heavy rare earths with about 30-at.% concentration, the system orders magnetically with magnetic wave vector $\vec{q}_m$ equal to $0.56\pi/c$.[7] It is generally assumed that the host metal scandium simply provides the medium for the indirect exchange interaction between the localized $f$ electrons situated on the rare-earth ions. While this may be so, the possibility of a spin-density wave developing in the system and supported by the exchange interaction between the conduction electrons cannot be ruled out. We have investigated such a possibility in a preliminary calculation in the following way. Following the work of Gupta and Sinha[1] on chromium, we make an ansatz for the form of the susceptibility matrix as follows,

$$\chi(\vec{q}+\vec{G},\ \vec{q}+\vec{G}') = f(\vec{q}+\vec{G})f(\vec{q}+\vec{G}')\bar{\chi}(\vec{q}) \ , \tag{21}$$

where $f(\vec{Q})$ is a function normalized to 1 at $\vec{Q}=0$. The actual form of $f(\vec{Q})$ is not important here since it does not enter into the calculation. It has been shown that the exchange-enhanced susceptibility is given by the expression

$$\chi_{\text{en}}(\vec{q},\vec{q}) = \chi(\vec{q},\vec{q})/[1 - IF(\vec{q})] \ , \tag{22}$$

where

$$F(\vec{q}) = \sum_{\vec{G}} \chi(\vec{q}+\vec{G},\ \vec{q}+\vec{G}) \ , \tag{23}$$

and $I$ is the strength of the exchange interaction (treated here in the usual $q$ independent approxi-

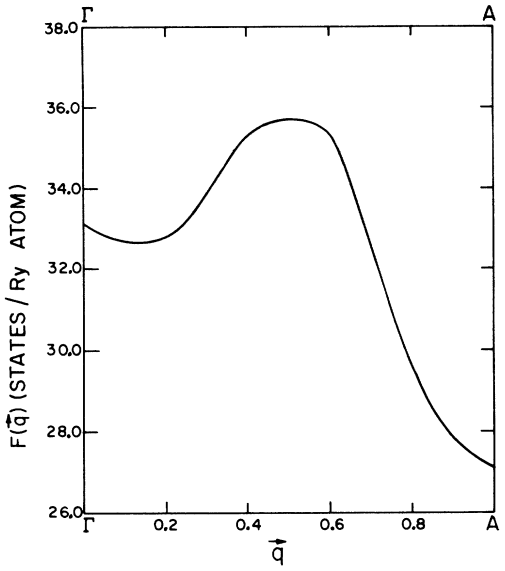


FIG. 11. Function $F(\vec{q})$ appearing in Eq. (23) and described in the text.

mation). Quite clearly, a spin-density wave may be sustained for a value of $\vec{q}$ for which $F(\vec{q})$ has a maximum. In the present work we have available $\chi(\vec{q}+\vec{G}, \vec{q}+\vec{G})$ for values of $\vec{q}+\vec{G}$ which are restricted to be along the $c$ direction and are not greater than $2\pi/c$. So if we make the crude approximation of restricting the sum over $\vec{G}$ to only a single reciprocal-lattice vector $2\pi/c$, then $F(\vec{q})$ is simply $\chi(\vec{q})+\chi(2\pi/c-\vec{q})$. This function is shown in Fig. 11. We find a broad peak at $\vec{q}\simeq 0.5\pi/c$, which is remarkably close to the value of the observed magnetic wave vector—especially in view of the very crude treatment given here.

## V. SUMMARY AND CONCLUSIONS

The generalized susceptibility function of a solid is rather cumbersome and difficult to evaluate computationally; hence, only scarce attention has been devoted for its proper evaluation. The so-called "constant matrix elements" approximation has been used frequently in $\chi(\vec{q})$ calculations which attempt to explain various phenomena such as the onset of spin-density waves and charge-density waves and to roughly account for the position of phonon anomalies. The argument for ignoring the oscillator-strength matrix elements in such calculations has been that the nesting features of the Fermi surface [i.e., the energy denominator in Eq. (3)] dominate over the influence of matrix elements and that the matrix elements are more or less smoothly and slowly varying functions of the vector $\vec{q}$. We have shown that these assumptions are far from being correct. Both the position and the shape of the peak arising from the nesting features of the Fermi surface were found to be strongly influenced by the oscillator-strength matrix elements.

In the case of scandium metal, it has usually been assumed that the peak in $\overline{\chi}(\vec{q})$ (i.e., in constant matrix elements approximation) results from nesting feature related to the third- and fourth-band part of the Fermi surface. Hence, one expects that such a nesting feature should yield even a sharper peak in the interband part of $\overline{\chi}(\vec{q})$ than that seen in $\overline{\chi}(\vec{q})$ itself. We found that upon decomposing the total contribution to $\overline{\chi}(\vec{q})$ into its intraband and interband parts, that the interband contribution did not have this expected peak. Instead, it was in fact the variation with respect to $\vec{q}$ of both intraband and interband parts which resulted in a sharp peak in $\overline{\chi}(\vec{q})$. This surprising result leads to the conclusion that the sharp peaks in $\overline{\chi}(\vec{q})$ may not be caused by any well-defined nesting features in the Fermi surface at all.

We have shown here that the matrix elements are very strongly dependent both on $k$ and $\vec{q}$, and it is not justified to ignore either the $k$ or the $\vec{q}$ dependence. For Sc metal, we have found the effect to be so overwhelming that the peaks in $\overline{\chi}(\vec{q})$ were washed out completely and no peaks are found in $\chi(\vec{q})$. One may well conclude that even in materials which do have sharp and well-defined nesting features in their Fermi surfaces, the influence of the matrix elements can be dramatic.

Although scandium metal itself is nonmagnetic, it becomes magnetic if alloyed with 30 at.% of, for instance, Tb with a magnetic wave vector $\vec{q}_m \approx (0, 0, 0.56\pi/c)$. This onset of magnetic behavior has always been interpreted in terms of local moments associated with the rare-earth-metal sites. The alternative possibility of the existence of a spin-density wave in the system has not been given serious consideration. By crudely including the local field corrections to obtain the exchange-enhanced susceptibility, we find that the possibility of a spin-density wave existing in scandium cannot be excluded. Since no spin-density wave has been observed in Sc metal, we believe that the exchange interaction in the pure metal is too weak. It is possible that the alloying with rare earths increases the strength of this interaction sufficiently to give rise to the formation of the spin-density wave in the system. Such a possibility should be examined by neutron scattering both for Sc and Y alloyed with dilute amounts of rare earths.

## ACKNOWLEDGMENT

We thank Dr. J. Rath for discussions on several aspects of this work.

*Supported by the AFOSR, the NSF through Northwestern University Materials Research Center, and the ERDA.

[1]R. P. Gupta and S. K. Sinha, Phys. Rev. B 3, 2401 (1971).

[2]J. F. Cooke, H. L. Davis, and M. Mostoller, Phys. Rev. B 9, 2485 (1974).

[3]An accurate calculation of $\epsilon(\vec{q},\omega)$, the dielectric function including local-field corrections, can be very helpful in resolving the controversy as to whether the anomalous behavior observed experimentally in $S(\vec{q},\omega)$ in Li, Be, and graphite is due to band-structure effects or many-body effects.

[4]W. M. Lomer, Proc. Phys. Soc. Lond. 80, 489 (1962).

[5]A. W. Overhauser, Phys. Rev. 128, 1437 (1962).

[6]J. Rath and A. J. Freeman, Phys. Rev. B 11, 2109 (1975).

[7]H. R. Child and W. C. Koehler, J. Appl. Phys. 37, 1353 (1966); Phys. Rev. 174, 562 (1968).

[8]N. Wakabayashi, S. K. Sinha, and F. H. Spedding, Phys. Rev. B 4, 2398 (1971).

[9]G. S. Fleming and T. L. Loucks, Phys. Rev. 173, 685 (1968).

[10]T. L. Loucks, *Augmented Plane Wave Method* (Benjamin, New York, 1967).

[11]M. H. Mueller (private communication).

[12]S. G. Das, A. J. Freeman, D. D, Koelling, and F. M. Mueller, AIP Conf. Proc. 10, 1304 (1973).

[13]W. E. Evenson and S. H. Liu, Phys. Rev. 178, 783 (1969).

[14]S. H. Liu, R. P. Gupta, and S. K. Sinha, Phys. Rev. B 4, 1100 (1971).

[15]M. E. Rose, *Elementary Theory of Angular Momentum* (Wiley, New York, 1957).

[16]S. K. Sinha, R. P. Gupta, and D. L. Price, Phys. Rev. B 9, 2564 (1974).

[17]D. L. Price, S. K. Sinha, and R. P. Gupta, Phys. Rev. B 9, 2573 (1974).

[18]S. K. Sinha and B. N. Harmon, Phys. Rev. Lett. 35, 1515 (1975).